THE JOURNAL OF PHYSICAL CHEMISTRY A

Article

pubs.acs.org/JPCA

Photoinduced Proton Coupled Electron Transfer in 2-(2′-Hydroxyphenyl)-Benzothiazole

Sandra Luber,[†,§] Katrin Adamczyk,[‡,∥] Erik T. J. Nibbering,*[,‡] and Victor S. Batista*[,†]

[†]Department of Chemistry, Yale University, P.O. Box 208107, New Haven, Connecticut, United States

[‡]Max-Born Institut für Nichtlineare Optik und Kurzzeitspektroskopie, Max Born Strasse 2A, 12489 Berlin-Adlershof, Germany

Supporting Information

ABSTRACT: We characterize the structural and electronic changes during the photoinduced enol−keto tautomerization of 2-(2′-hydroxyphenyl)-benzothiazole (HBT) in a nonpolar solvent (tetrachloroethene). We quantify the redistribution of electronic charge and intramolecular proton translocation in real time by combining UV-pump/IR-probe spectroscopy and quantum chemical modeling. We find that the photophysics of this prototypical molecule involves proton coupled electron transfer (PCET), from the hydroxyphenyl to the benzothiazole rings, resulting from excited state intramolecular proton transfer (ESIPT) coupled to electron transfer through the conjugated double bond linking the two rings. The combination of polarization-resolved mid-infrared spectroscopy of marker modes and time-dependent density functional theory (TD-DFT) provides key insights into the transient structures of the molecular chromophore during ultrafast isomerization dynamics.

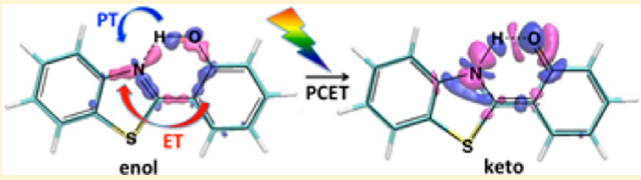

1. INTRODUCTION

Understanding the coupling between electronic and nuclear rearrangements of photoinduced proton transfer mechanisms is central to emerging technologies ranging from optical data storage,[1] optically controlled molecular switching,[2,3] molecular electronic logic gates,[1] and molecular nanotechnology,[2] including molecular motors,[4−6] molecular sensors,[7] and receptors.[1] Monitoring the underlying ultrafast relaxation processes in real time, however, is challenging and requires state-of-the-art spectroscopic techniques made available only in recent years. Here, we combine polarization-resolved femtosecond infrared spectroscopy and computational modeling to study the ultrafast proton coupled electron transfer dynamics associated with the photoinduced enol−keto tautomerization of 2-(2′-hydroxyphenyl)-benzothiazole (HBT). We obtain the vibrational fingerprint patterns (including anisotropies) of the transient states by use of polarization sensitive femtosecond infrared spectroscopy, and we explore marker bands of local vibrational modes providing direct insight into structural rearrangements due to proton transfer coupled to redistribution of electronic density. Pump−probe measurements are correlated with calculations of ground and excited electronic state infrared spectra, probing the evolution of photoinduced intramolecular proton coupled to electron transfer. Some of the fundamental questions resolved by the reported studies are as follows: What kind of excited state conformational changes are triggered by photoexcitation? Does photoinduced proton transfer induce cis/trans isomerization of the proton donor−acceptor moieties with picosecond twisting motion around the interaromatic single bond[8] or maintain coplanarity of the molecule? What is the effect of conformational changes on the subsequent dynamics? What is the influence of the surrounding molecular environment (e.g., the nonpolar solvent) on the transient state structures?

A variety of methods have been developed to address nuclear and electronic rearrangements in short-lived excited electronic states of polyatomic systems since the advent of short pulse laser technology.[9] In particular, time-resolved electronic spectroscopy has been widely applied in conjunction with computational modeling and the relaxation dynamics of electronic excited states has been investigated in many chemical and biological systems. In addition, ground state proton-coupled electron transfer (PCET) has been studied in certain molecules.[10−23] A technical challenge for ultrafast PCET in electronic excited states is that electronic spectroscopy provides limited structural detail for condensed phase molecular systems. This is due to the large spectral broadening, typical of strong solute−solvent couplings. Here, we bypass these limitations by implementing ultrafast vibrational spectroscopy to monitor structure-specific marker modes during the reaction dynamics.[24,25]

After earlier pioneering work,[26−28] ultrafast vibrational spectroscopy has become an important tool to follow chemical reactions. Bond cleavage of metallocarbonyl compounds,[29,30] ligand dissociation in heme proteins,[27,31−34] twisting of side groups,[35−41] and trans/cis isomerization[42−54] are examples of photoinduced rearrangements of chemical bonds that have been probed by ultrafast infrared (IR) and Raman spectroscopy. Other examples include electron[55−58] and proton[59−67] transfer investigated with ultrafast vibrational spectroscopy.

Received: April 4, 2013
Revised: May 25, 2013
Published: May 29, 2013

   dx.doi.org/10.1021/jp403342w | J. Phys. Chem. A 2013, 117, 5269−5279

We focus on PCET in HBT probed through the analysis of the IR-active vibrational fingerprint modes (Figure 1). In nonpolar solvents, HBT in the electronic ground state is stabilized in the enol form by an intramolecular hydrogen bond between the hydroxyphenyl and benzothiazole rings.

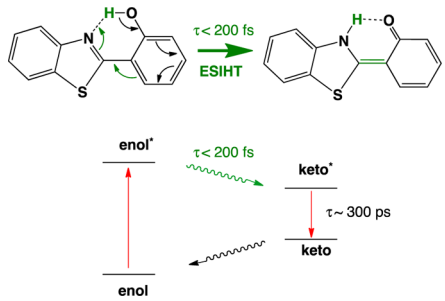

Figure 1. Photocycle of HBT, including photoexcitation and excited state intramolecular PCET.

Electronic excitation triggers excited state intramolecular proton transfer (ESIPT) in the S_1 state, concerted with electron transfer, forming the keto isomer on ultrafast time scale.[26,68,69] As shown by UV/vis electronic spectroscopy and theoretical studies, the ESIPT process is faster than 200 fs and involves wavepacket motions of Raman-active vibrations modulating the intramolecular hydrogen bond distance.[70,71] These earlier spectroscopic and theoretical studies[71−77] have gathered much information on the photophysics of HBT and related molecular systems.[78−80] However, the underlying mechanism driving the ultrafast PCET process remains poorly understood. In fact, it remains unclear whether PCET induces cis/trans isomerization of the proton donor−acceptor moieties or keeps the system in a coplanar configuration. Furthermore, it is unclear whether the process involves ESIPT or excited state intramolecular hydrogen transfer (ESIHT).[79] Apart from resolving these fundamental aspects, understanding the underlying structural rearrangements is of much interest for technological applications. HBT and its derivatives have already raised significant interest in applications to organic light emitting diodes (OLEDs),[81,82] molecular sensors[62] and receptors, optical data storage,[1] and optically controlled molecular switching,[2,3] in addition to applications as ligands in organic chelate metal complexes.[81,83−88] In Zn complexes, HBT derivatives have already been shown to form outstanding electroluminescent materials.[81,85,86,88] HBT-containing OLEDs can thus be designed by modification of HBT[88−93] as well as by exchange of metal atoms in the complexes.[90,92]

In this study, we combine polarization-resolved ultrafast mid-IR absorption measurements and computational modeling to monitor the frequencies and anisotropies of the IR-active fingerprint modes characterizing PCET in HBT. The analysis of excited state vibrational fingerprint patterns is based on time-dependent density functional theory (TDDFT) which has been successfully applied in earlier studies of ESIPT,[75] and in other studies of excited state normal-mode analysis.[80,94−97] Due to the moderate computational cost (as reviewed in refs 98 and 99), the method is more practical than complete active space self-consistent field (CASSCF) calculations[100] and comparable to configuration interaction with singles (CIS)[37,40,101,102] which has been used to determine, for example, whether vibrational mode patterns provide insight into twisting or planarization mechanisms of the NH_2 group in dimethylaminobenzonitrile, or possible twisting dynamics in the chromophore of green fluorescent protein. Analogously, the TDDFT analysis provides a detailed understanding of the keto-S_1 state in terms of electronic charge distributions and nuclear rearrangements affecting the vibrational fingerprint.

The manuscript is organized as follows. Section 2 introduces the experimental and computational methods implemented to analyze PCET in HBT and to address the orientation of fingerprint modes by probing the frequencies and anisotropies of the IR-active transitions.[27,31−33,45,102−104] The comparison of experimental and calculated IR spectra is presented in section 3, followed by a discussion of the structural dynamics insights that emerge from the analysis of anisotropies in section 4. After the analysis and discussion of the electronic and structural rearrangements in section 5, we summarize and conclude in section 6.

2. METHODS

This section describes the experimental and theoretical methods applied to study photoinduced PCET in HBT through the analysis of fingerprint vibrational modes and anisotropies that respond to specific nuclear and electronic rearrangements during the course of the reaction.

2.1. Femtosecond Transient Infrared Spectroscopy. Polarization-sensitive ultrafast IR spectroscopy allows one to probe the fingerprint patterns and vibrational anisotropies of short-lived transient states during ultrafast reaction dynamics, since the linearly polarized UV/vis pump pulse preferentially excites molecules that are oriented along the polarization direction of the beam. The measured quantity is the ensemble-averaged anisotropy $\alpha(\tau)$ of the transient IR absorption with respect to the polarization direction of the visible pump pulse (for details, see refs 105 and 106)

$$\alpha(\tau) = \frac{2}{5}\langle P_2[\hat{\mu}_2(\tau)\cdot\hat{\mu}_1(\tau = 0)]\rangle \tag{1}$$

where $\langle\cdots\rangle$ represents an ensemble average over all molecular orientations (we omit the dependence of $\alpha(\tau)$ on the excitation and observation frequencies). In eq 1, $P_2(x) = (3x^2 - 1)/2$ is the second-order Legendre polynomial, while τ is the pulse delay, with $\tau = 0$ defined as the time of the pump-pulse. In addition, $\hat{\mu}_1(\tau)$ and $\hat{\mu}_2(\tau)$ are the electronic and vibrational transition dipole moments, respectively.

The anisotropy measure $\alpha(\tau)$ thus contains information about the orientation of the transition dipole moment $\hat{\mu}_2(\tau)$ of the vibrational normal mode under consideration, since the second-order Legendre polynomial

$$\langle P_2[\hat{\mu}_2(\tau)\cdot\hat{\mu}_1(0)]\rangle = \frac{1}{2}\langle[3\cos^2(\theta(\tau)) - 1]\rangle \tag{2}$$

yields the anisotropy angle $\theta(\tau)$ between $\hat{\mu}_2(\tau)$ and the electronic transition dipole moment $\hat{\mu}_1(\tau = 0)$. Therefore, the anisotropy at a specific frequency provides the time-dependent orientation of the absorber mode from the angle $\theta(\tau)$ between the vibrational transition dipole moment $\hat{\mu}_2(\tau)$ and the electronic transition dipole moment $\hat{\mu}_1(\tau)$.[102,105,107]

Our experiments involve femtosecond UV-pump/IR-probe spectroscopy on HBT dissolved in C_2Cl_4 (Aldrich, pro analyze).[30,64] In short, parametric frequency conversion of the output of an amplified Ti:sapphire laser system is used to generate 50 fs UV-pump pulses tuned at 330 nm with 2−3 μJ pulse energies and 100 fs tunable mid-IR probe pulses, focused to the sample with spot sizes of 200 μm diameter. Transient

mid-IR spectra are recorded using a polychromator and a HgCdTe mid-IR diode array. The sample solutions are pumped through a 100 μm thick flow cell, using 1 mm thick BaF_2 windows. Group velocity mismatch between UV-pump and IR-probe pulses is the main factor for the effective time resolution of 150 fs.

Figure 2 shows transient HBT spectra recorded at delay times of −1, +0.3, and +100 ps relative to the pump pulse. In

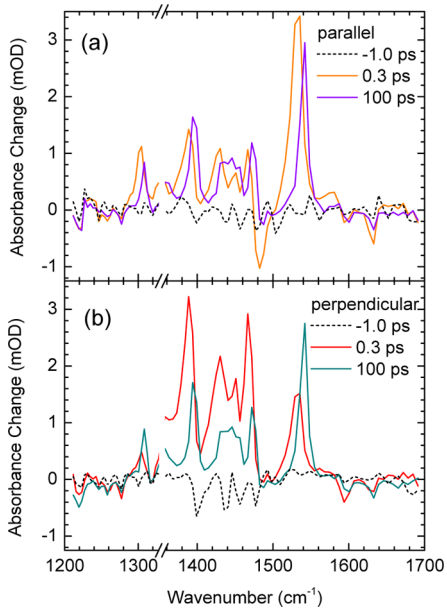

Figure 2. Transient IR spectra of HBT dissolved in C_2Cl_4 measured at specific pulse delays for parallel (a) and perpendicular (b) polarization conditions of UV-pump and IR-probe pulses.

the spectrum recorded at negative pulse delay (i.e., −1 ps), only bleach signals are present, indicative of the HBT enol-S_0 state due to perturbed free induction decay contributions,[108−110] with which we can determine the anisotropy of selected vibrations of HBT in the enol-S_0 state. Much larger signals appear at positive pulse delays due to the transiently generated HBT in the keto-S_1 state. We have analyzed the fingerprint patterns using our measurements recorded at long pulse delay (i.e., 100 ps).

In the determination of the frequencies and anisotropies of fingerprint marker modes, we take into account possible spectral overlap between ground state bleach and excited state absorption signals. In addition, intramolecular vibrational redistribution leads to vibrational excess energy in the keto-S_1 state at early pulse delay.[111,112] Upon vibrational cooling on picosecond time scales, the fingerprint modes exhibit a vibrational frequency upshift on the order of 2−7 cm^{-1}. Such frequency shifts may affect the early time dynamics of the pump−probe signals, leading to a different degree of spectral overlap as exemplified by the weak band at 1587 cm^{-1} of the keto-S_1 state that is more prominent at early pulse delays than at later times when it overlaps more with the 1600 cm^{-1} enol-S_0 state ground state bleach (see Figure 3).

During the course of the reaction, $\theta(t)$ may change as the nature of the vibrational marker modes changes. However, we focus on the early time dynamics while the polarization-resolved spectra are mostly affected by vibrational cooling, resulting in small frequency up-shifts and rotational diffusion with a time constant of 30 ps (Figure 4), leading to changes in

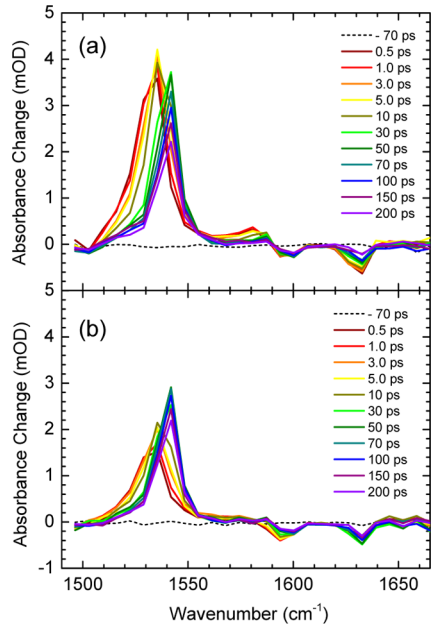

Figure 3. Transient IR spectra measured at early pulse delays for parallel (a) and perpendicular (b) polarization conditions of UV-pump and IR-probe, showing the effects of vibrational cooling and rotational diffusion on the fingerprint modes.

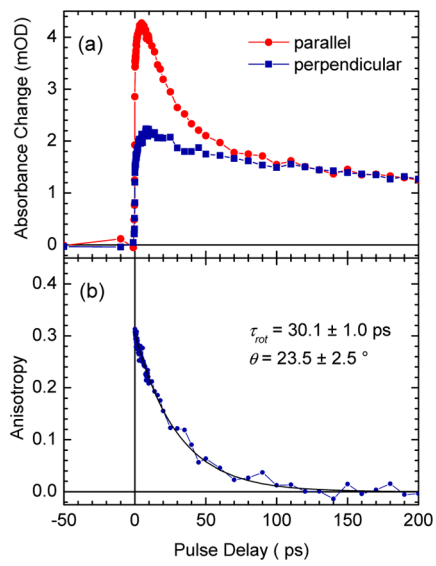

Figure 4. (a) Polarization-dependent kinetics of the 1542 cm^{-1} marker mode of HBT in the keto-S_1 state and (b) derived anisotropy $\alpha(\tau)$ showing the effect of rotational diffusion.

signal strengths depending on the anisotropy. We determine the anisotropy as a function of the pulse delay τ

$$\alpha(\tau) = \frac{S_{\parallel}(\tau) - S_{\perp}(\tau)}{S_{\parallel}(\tau) + 2S_{\perp}(\tau)} = \frac{1}{2}[3\cos^2(\theta(\tau)) - 1]\frac{2}{5}e^{-\tau/\tau_{rot}} \quad (3)$$

where $S_{\parallel}(\tau)$ and $S_{\perp}(\tau)$ are the transient absorbance signals for parallel and perpendicular polarization and τ_{rot} is the rotational diffusion time constant. For robustness of our analysis, we extrapolate the anisotropy back to zero time-delay to determine $\alpha(\tau = 0)$ and $\theta(\tau = 0)$ while they are still unaffected by rotational diffusion.

Tables 1 and 2 summarize the resulting values of frequencies and anisotropies obtained from the measurements of absorbance changes and anisotropies shown in Figures 3 and 4.

Table 1. Measured and Calculated Anisotropy Angles θ of Selected Experimental Bands/Calculated Normal Modes Ω of Cis−Enol in the Ground State[a]

Ω (cm^{-1})		θ (deg)	
exp.	theory	exp.	theory
1491/1496	1500	10 ± 10	9
1594/1600	1572	65 ± 10	63
1594/1600	1578	65 ± 10	41
1633	1610	12 ± 12	11

[a]Vibrational transition dipole moments: DFT (BP86/TZVP/PCM). Electronic transition dipole moment: TDDFT(B3LYP/TZVP/PCM).

2.2. Computational Modeling. Computational structural models of the cis−enol, cis−keto, and trans−keto isomers (Figure 5) in the S_0 and S_1 electronic states were prepared by DFT geometry optimization. Solvation effects due to tetrachloroethene were modeled via the solvent continuum model PCM,[113] as implemented in Gaussian 09.[114]

Normal modes, frequencies, and IR intensities as well as anisotropy angles θ of specific normal modes were obtained with a modified and extended version of the SNF package.[115,116] The BP86[117] and B3LYP[118,119] density functionals in combination with Ahlrichs' TZVP[120,121]/TZVPP[121,122] basis sets were employed for the calculation of ground- and excited state IR spectra, respectively. For comparison, we also performed calculations based on the CIS/TZVP and second-order coupled cluster CC2/TZVP methods, as implemented in Turbomole.[123] The best agreement with experiments was obtained at the TDDFT level. Electronic energy gradients and electric dipole moments were computed with Gaussian 09, and the data were collected by SNF to evaluate the normal modes and IR intensities. Differentiation was performed by using a three-point central difference formula[124] with a finite increment differentiation step of 0.01 bohr. Electrostatic-potential (ESP) atomic charges were computed according to the Merz−Singh−Kollman[125,126] scheme, as implemented in Gaussian 09. Electronic transition dipole moments for $S_1 \leftarrow S_0$ photoexcitation were obtained at the TDDFT level with the density functional B3LYP and the TZVP or TZVPP basis sets as implemented in Gaussian 09. Molecular structures and normal modes were visualized by using the programs Vmd[127] and Jmol,[128] respectively.

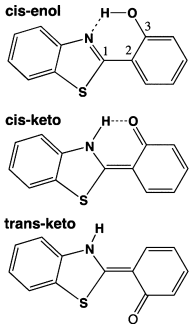

Figure 5. Structures of HBT, including the enol and keto (cis and trans) discussed in the text.

3. EXCITED STATE IR SPECTRA

Figure 6 compares the calculated spectra for the S_1 trans−keto* (a) and cis−keto* (b) isomers of HBT to the transient IR spectrum measured at 100 ps after UV excitation (c). Due to partial cancellation of the excited state signals with bleaching vibrational bands of the cis−enol S_0 state, panels d and e, the intensities are difficult to correlate. However, the positions of the transient bands are in very good agreement with the calculated vibrational modes for the cis−keto* state.

For example, the peak at 1305 cm^{-1} is in accordance with the calculated band at ∼1309 cm^{-1} for the C—H rocking and C—C stretching vibrations (Figure 7). Also, the most intense experimental band at 1542 cm^{-1} corresponds to the calculated normal mode at 1540 cm^{-1} including C═O, C—C stretching, C—H bending and rocking vibrations, mostly on the quinone ring. Furthermore, the broad experimental band in the 1430−1460 cm^{-1} range correlates nicely with the two normal modes at 1435 and 1439 cm^{-1}, showing C—H rocking vibrations in the benzothiazole and quinone rings, respectively. Finally, the experimental band at 1475 cm^{-1} corresponds to the calculated mode at 1471 cm^{-1} associated with the mixture of in-plane C—H, C—C, and carbonyl stretching vibrations of the quinone ring (Figure 7). The only band in disagreement is the peak at 1397 cm^{-1} that is apparently shifted to 1383 cm^{-1}. However, this band might be a combination or overtone band, as suggested by the analysis of anisotropies (*vide infra*). In addition, peaks at 1267, 1582, 1601, and 1612 cm^{-1} are missing in the pump−probe signal due to cancellation with bleaching S_0 bands.

In contrast to the spectrum of the cis−keto* isomer (Figure 6b), the computed spectrum of the trans−keto* form (Figure 6a) shows less agreement with experimental data (Figure 6c). This observation partially supports the finding that the cis−keto* form is the dominant product of photoinduced PCET in the first electronically excited state of HBT.[26,69] Nevertheless,

Table 2. Measured and Calculated [TDDFT (B3LYP/TZVPP)] Anisotropy Angles θ of Selected Experimental Bands/Calculated Normal Modes Ω of Cis−Keto and Trans−Keto in the First Electronically Excited State

Ω (cm^{-1})		θ (deg)	
exp.	theory cis−keto* (trans−keto*)	exp.	TDDFT cis−keto* (trans−keto*)
1305	1309 (1301)	29 ± 5	23 (6)
1397	673 + 736 (685 + 727)	90 − 15	90 (90)
1439	1439 (1433)	77 ± 13	77 (34)
1475	1471 (1472)	90 − 15	65 (79)
1475	1480 (1488)	90 − 15	71 (39)
1542	1540 (1523)	23.5 ± 2.5	26 (28)

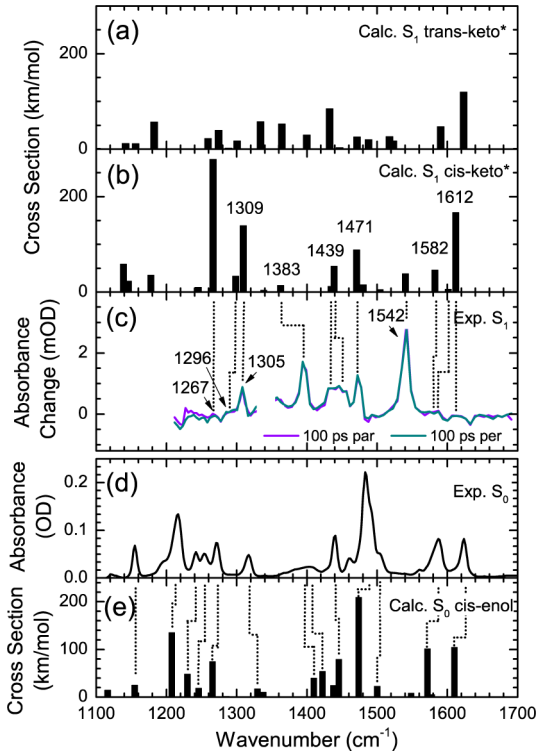

Figure 6. Spectra of HBT in the S_1 state in the trans−keto* (a) and cis−keto* (b) configurations, calculated with TDDFT (B3LYP/TZVPP), and compared to the transient IR spectrum measured at 100 ps pulse delay after excitation at 330 nm (c). The steady state IR spectrum of HBT in C_2Cl_4 (d) is compared to the spectrum calculated at the DFT (BP86/TZVP/PCM) level (e) for HBT in the cis−enol configuration of the S_0 state.

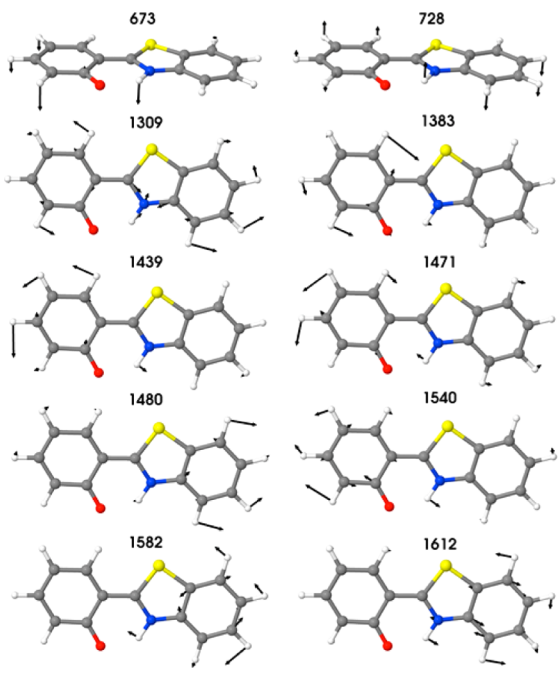

Figure 7. Graphical representation of selected fingerprint normal modes of cis−keto* [TDDFT(B3LYP/TZVPP)] with the corresponding wavenumbers in cm^{-1}.

we emphasize that the analysis of the frequencies alone cannot rule out formation of trans−keto*, since most of the bands of that isomer are similar to those of the cis−keto* form. For example, the experimental band at 1305 cm^{-1} is also found in the trans−keto* spectrum, resulting from a normal mode at 1301 cm^{-1}. The normal mode computed at 1400 cm^{-1} may give rise to the experimental band at 1397 cm^{-1}, and several normal modes having frequencies in good agreement with the experimental bands are computed for the 1430−1480 cm^{-1} range. The most conspicuous difference between the calculated cis−keto* and trans−keto* excited state IR spectra, however, is the band belonging to the carbonyl stretching vibration, observed in experiments at around 1542 cm^{-1} and computed for cis−keto* at 1540 cm^{-1}. For trans−keto*, however, only a weak band is obtained and with a lower wavenumber (1523 cm^{-1}). Other differences include the normal modes in the 1330−1370 cm^{-1} range, showing high IR absorbance in contrast to the corresponding cis−keto* normal modes and the experimental data. Therefore, we conclude the fingerprint analysis is more consistent with the HBT S_1 population in the cis−keto* state than in the trans−keto* state generated by cis/trans isomerization upon rotation of the quinone and benzothiazole moieties relative to each other along the connecting CC bond, as discussed for the ground state[48] as well as for other similar systems.[8] Resolving the cis−keto* versus trans−keto* issue, however, requires the analysis of anisotropies.

4. ANISOTROPIES

The anisotropy angle θ between the vibrational and electronic transition dipole moments provides information on the orientation of the normal mode as quantified by its perturbation on the orientation of the molecular dipole moment with respect to the electronic transition dipole moment. As described before, it is obtained from the internal product of the electronic transition dipole moment of the system and the vibrational transition dipole moment (i.e., dipole moment change per unit displacement along the normal mode of interest).

Table 1 reports the comparison of calculated and experimental anisotropy angles θ for various vibrational bands of HBT in the S_0 cis−enol state. We show that the 1495 cm^{-1} band has an anisotropy angle of $\theta = 10 \pm 10°$ in very good agreement with the value $\theta = 9°$ obtained from quantum chemistry calculations. Two normal modes at 1572 and 1578 cm^{-1} may contribute to the experimental band at 1597 cm^{-1}, since the anisotropy angle corresponding to the 1572 cm^{-1} component agrees very well with the experimental value. Furthermore, the calculated anisotropy angle of 11° for the normal mode at 1610 cm^{-1} is also in line with the experimental value of $12 \pm 12°$. This consensus between experimental and calculated anisotropy angles supports not only the quantum chemistry procedure for calculations of θ but also the assignment of fingerprint bands. Furthermore, these results show that the TDDFT electronic transition dipole moments are reliable and allow for predictions of anisotropy angles.

Table 2 shows the comparison of calculated and experimental anisotropies for the S_1 cis−keto* state. The experimental value of $29 \pm 5°$ for the band at 1305 cm^{-1} is reproduced by the calculated value of 23° for the normal mode at 1309 cm^{-1}. An exception to this agreement is the band at 1397 cm^{-1} with an anisotropy angle of $90 - 15°$. The computed anisotropy values for the closer normal modes at 1383, 1363, and 1435 cm^{-1} are very different (e.g., 11, 3, and 14°, respectively). As mentioned in the previous section, this

disagreement suggests that the 1397 cm^{-1} band arises from combination or overtone bands. According to the calculated IR spectrum, we find that the normal modes at 673, 705, 728, 736, and 746 cm^{-1} lead to an anisotropy angle of 90° whereby especially the ones at 673, 736, and 746 cm^{-1} show also a high IR absorbance. Thus, a combination band resulting from the normal modes at 673 and 736 cm^{-1} may be the reason for the high θ value measured in experiments. The experimental band at 1439 cm^{-1} with an anisotropy angle of 77 ± 13° is easily assigned to the calculated normal mode with the same wavenumber leading to exactly 77°. The computed normal modes at 1471 and 1480 cm^{-1} with anisotropy values of 65 and 71°, respectively, reproduce quite well the experimental 90 − 15° for the band at 1475 cm^{-1}. A very good agreement is also obtained for the prominent experimental band at 1542 cm^{-1} and the calculated normal mode at 1540 cm^{-1} with values of 23.5 ± 2.5 and 26°, respectively. It is important to emphasize, however, that the size of the basis set is critical for this agreement. In fact, anisotropies obtained with the smaller TZVP basis set do not show the level of agreement with experimental data, as shown in Table 1 for the larger TZVPP basis set.

As discussed in the previous section, the comparison of calculated and experimental S_1 IR spectra did not allow one to determine whether the photoinduced PCET induces cis/trans isomerization and generates a mixture of cis−keto* and trans−keto* isomers in the excited state or if one of the two isomers is the predominant excited state component. Here, we show that the comparison of anisotropy angles clearly resolves this fundamental problem.

Table 2 also compares the anisotropy angles θ for selected vibrational bands of the trans−keto* states to show much better agreement with experiments for the cis−keto* bands than for the trans−keto* isomer. For example, the experimental band at 1305 cm^{-1} has an anisotropy of 29 ± 5°, while the corresponding trans−keto* band (at 1301 cm^{-1}) has an anisotropy of 6°. In contrast, the 23° anisotropy of the corresponding band for the cis−keto* isomer (at 1309 cm^{-1}) is in much better agreement with experiments. Another example is the normal mode at 1439 cm^{-1} with anisotropy of 77° in quantitative agreement with the frequency and anisotropy of the corresponding band for the cis−keto* isomer. In contrast, the corresponding band for the trans−keto* state (at 1433 cm^{-1}) has an anisotropy of 34° significantly different from the experimental value. Similarly, the experimental band at 1475 cm^{-1} has an anisotropy of 90° in much better agreement with the corresponding band for the cis−keto* band at 1480 cm^{-1} with an anisotropy angle of 79° than for the corresponding mode of the trans−keto* state at 1480 cm^{-1} with an anisotropy angle of 39°. In summary, the calculated wavenumbers and anisotropy angles of trans−keto* show a larger deviation from the experimentally derived values than those evaluated for the cis−keto*. This supports the conclusion that cis−keto* is the product of intramolecular PCET, a process that does not induce out-of-plane rotation of the benzothiazole proton acceptor relative to the phenol/quinone proton donor. These findings are consistent with earlier studies of the dynamics of HBT where the cis−keto* isomer was favored as the main reaction product in nonpolar solution.[24,59,60,62,63,67,101,102] However, for the first time, our anisotropy data shows that formation of trans−keto* can be excluded as an outcome of the isomerization of HBT in C_2Cl_4. These results demonstrate the capabilities of our approach based on the analysis of polarization-resolved ultrafast infrared spectroscopy for resolving the possible involvement of the twisting coordinate during PCET. The resulting insight is consistent with the shorter lifetime of the S_1 state for HBT in the gas phase,[73] the observed transient trans−keto product in the S_0 state in acetonitrile,[48] and analogous observations for HBO.[129,130]

5. ELECTRONIC AND NUCLEAR CHANGES DUE TO PCET

The photoinduced PCET dynamics in HBT involves structural rearrangements associated with breaking the OH bond in the phenyl moiety, and electron transfer to the benzothiazole to form the NH bond (Figure 1). To quantify these changes, we first discuss the structural changes of the cis−enol as it gets photoexcited from the ground state to the S_1 state, and then the changes due to conversion into the cis−keto* in the excited S_1 state. In accordance with ref 72 and contrary to ref 75, we find an energy minimum for cis−enol in the S_1 state. Table 3 and

Table 3. Calculated Bond Lengths [(TD)DFT(B3LYP/TZVP/PCM)] of Cis−Enol in the Ground and Excited States as Well as Cis− and Trans−Keto* and Cis−Keto

bond length (Å)	cis−enol	cis−enol*	cis−keto*	trans−keto*	cis−keto
$N-C_1$	1.304	1.356	1.357	1.367	1.335
C_1-C_2	1.453	1.418	1.449	1.444	1.413
C_2-C_3	1.420	1.467	1.467	1.463	1.458
C_3-O	1.346	1.319	1.275	1.268	1.277
O−H	0.991	1.037	1.805	4.760	1.543
N−H	1.741	1.583	1.032	1.008	1.076

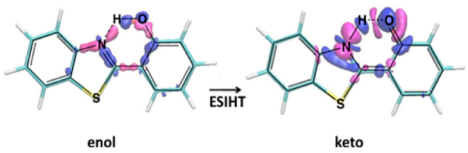

Figure 8. Electron density differences cis−enol*-*minus*-cis−enol (left) and cis−keto*-*minus*-cis−enol* (right). Blue: electron difference density at −0.003 e/bohr^3 (left, e is the charge of the electron) and −0.005 e/bohr^3 (right). Magenta: 0.003 e/bohr^3 (left) and 0.005 e/bohr^3 (right).

Figure 8 shows that there are significant differences in the structure of cis−enol* already when compared with the ground state cis−enol. The $N-C_1$ bond (for the numbering of atoms, see Figure 5) in the S_1 state becomes longer, whereas the C_1-C_2 distance gets shorter (compare the bond lengths in Table 3), consistent with the double bond formed by photoexcitation. Analogously, the neighboring C_2-C_3 bond in the phenol ring deviates from its equilibrium value due to elongation by 0.047 Å and an increasing double-bond character is observed for the C_3-O bond due to shortening by 0.027 Å. The N−H distance of cis−enol* is already significantly shortened by 0.158 Å, compared to cis−enol in the ground state, and the O−H bond is slightly longer. These changes facilitate PCET with a net hydrogen transfer from the oxygen donor to the nitrogen acceptor.

The $N-C_1$ and C_2-C_3 bonds remain almost unchanged during the cis−enol* to cis−keto* transformation. However, the C_1-C_2 bond is lengthened in the cis−keto* state,

facilitating the formation of twist excited state keto forms, as suggested in ref 73. For the C−O bond, a further shortening is obtained during formation of the carbonyl group. The hydrogen bond length, scaling with the sum of the O−H and N−H bonds, is indicative of the hydrogen bond strength. From the calculations, we learn that this sum decreases by 0.11 Å upon excitation from cis−enol to cis−enol*, and then increases again by 0.22 Å when cis−keto* is generated. This shows again that the optical excitation induces electronic charge redistribution and prepares HBT in a state that facilitates the intramolecular hydrogen transfer.

For completeness, bond lengths of the trans−keto* and cis−keto isomers are also given in Table 3. We note that the N—C_1, C_1—C_2, and C_2—C_3 bonds are shorter in the cis−keto state than in the cis−keto* configuration, in agreement with ref 72. It is worth mentioning that the C_1—C_2 bond length in the cis−enol* state is similar to the corresponding double bond length in cis−keto. In addition, the N—C_1, C_1—C_2, and C_2—C_3 bond lengths are similar in the trans−keto* and cis−keto* states. The electronic changes occurring during the electronic excitation and the subsequent enol−keto transformation are visualized in Figure 8. The left-hand side of Figure 8 shows the change in electron densities due to the cis−enol* ← cis−enol excitation. The magenta and blue isosurfaces show regions where the electron density is respectively increased and decreased upon excitation. We note that the electron density centered on the N—C_1, C_2—C_3, and O—H bonds is reduced upon excitation to the S_1 state, according to elongation of these bonds as presented in Table 3. Similarly, a higher electron density is computed for the shortened C_1—C_2 and C—O bonds as well as on the N atom, thus raising its base character. The higher double-bond character of the C═O bond and the weakened O—H bond in cis−enol* support an enhancement of the acidity of the phenol group. The right-hand side of Figure 8 shows the changes from cis−enol* to cis−keto* due to formation of the N—H bond and the C═O double bond, visualized by the increased electron density (magenta) as well as the increased electron density upon formation of the additional lone pair in O of the carbonyl group.

Comparing the ESP charges of cis−enol* to those of cis−enol, lower charges are obtained for the N, C_2, and O atoms, whereas higher ESP charges are calculated for H, C_3, and C_1. These findings show that the excitation of cis−enol to the S_1 state leads to electronic changes that favor intramolecular PCET. However, it is important to note that no net charge is transferred from phenol to benzothiazole during the electronic excitation, since the sum of ESP charges for the phenol (0.13 q_e with q_e being the elementary charge) and benzothiazole (−0.13 q_e with q_e being the elementary charge) remains almost unchanged.

A small amount of positive charge is transferred to benzothiazole when cis−enol* converts into cis−keto*. Specifically, the benzothiazole charge difference is about 0.34 q_e (i.e., only 34% of a full proton transfer) upon excited state enol−keto tautomerization, with cis−enol* −0.13 q_e and cis−keto* 0.21 q_e. According to these results, we conclude that the photoinduced PCET in HBT should be described as excited state intramolecular hydrogen transfer, i.e., ESIHT, rather than the traditional ESIPT, with the proton transfer through-space concerted with electron transfer through a conjugated double bond.

■ SUMMARY AND CONCLUSIONS

We have combined experimental and computational methods to characterize the dynamics of PCET in HBT due to photoinduced keto−enolic tautomerization in the S_1 state. The methodology involves UV-pump/IR-probe spectroscopy and quantum chemical modeling, allowing us to quantify the redistribution of electronic charge coupled to intramolecular proton translocation in real time. An essential advantage of this approach is the analysis of anisotropy angles for fingerprint modes from both the ground and excited state IR spectra. The vibrational anisotropies provide valuable information on the orientation of vibrational transition dipole moments, with respect to the electronic transition dipole moment, that are sensitive to proton and electron transfer.

We find that the calculated vibrational properties of the cis−keto* isomer are in much better agreement with experimental data than the corresponding vibrational features of the trans−keto* form. These results suggest that PCET does not involve cis/trans isomerization with out-of-plane twisting motion, as suggested for similar systems, but rather maintains coplanarity of the molecule as in HBO,[129,130] ensuring in-plane net hydrogen transfer from phenol to benzothiazole.

Our quantum chemical analysis shows that the $S_1 \leftarrow S_0$ electronic excitation of cis−enol HBT leads to nuclear and electronic changes that facilitate hydrogen transfer. Certain bonds show a pronounced double-bond character, while the N−H bond becomes shorter, already in the cis−enol* form, as observed in the cis−keto* structure. However, no net charge is transferred from the phenol to the benzothiazole part during the cis−enol electronic excitation.

Looking at the cis−keto* isomer, we find that the bond lengths of N—H and C═O are similar to those of cis−keto in the ground state. These results are consistent with functional groups that remain neutral due to the simultaneous proton transfer coupled to redistribution of electronic charge in the enol−keto isomerization. The resulting PCET of cis−enol* to cis−keto* is thus described as ESIHT, instead of the traditionally used ESIPT. These findings demonstrate that ultrafast polarization-sensitive mid-IR measurements provide a powerful method for the study of photoexcited PCET when combined with TDDFT calculations. The data provide a profound understanding of both electronic and nuclear rearrangements in the excited state. The methodology can be straightforwardly applied to the analysis of ultrafast PCET in other molecules. Therefore, it should be particularly valuable for the characterization and optimization of molecular photoswitches.

■ ASSOCIATED CONTENT

Supporting Information

Detailed computational procedure. IR spectra of HBT in the S_1 state with cis−keto* configuration, calculated at various level of theory and compared to the transient IR spectrum measured at 100 ps pulse delay. Comparisons of experimental and calculated anisotropy angles of selected bands and normal modes of HBT cis−keto and trans−keto in the first electronically excited state. This material is available free of charge via the Internet at http://pubs.acs.org.

AUTHOR INFORMATION

Corresponding Author

*E-mail: nibberin@mbi-berlin.de (E.T.J.N.); victor.batista@yale.edu (V.S.B.).

Present Addresses

[§]University of Zurich, Winterthurerstrasse 29, 8057 Zurich, Switzerland.

[‖]Department of Physics, University of Strathclyde, 107 Rottenrow, Glasgow G4 0NG, U.K.

Notes

The authors declare no competing financial interest.

ACKNOWLEDGMENTS

V.S.B. acknowledges financial support by the National Science Foundation (Grant CHE 0911520) and supercomputer time from NERSC and from the High Performance Computing facilities at Yale University.

REFERENCES

(1) Feringa, B. L. *Molecular Switches*; Wiley-VCH: Weinheim, Germany, 2001.

(2) Tamai, N.; Miyasaka, H. Ultrafast Dynamics of Photochromic Systems. *Chem. Rev.* **2000**, *100*, 1875−1890.

(3) Berkovic, G.; Krongauz, V.; Weiss, V. Spiropyrans and Spirooxazines for Memories and Switches. *Chem. Rev.* **2000**, *100*, 1741−1754.

(4) Dugave, C.; Demange, L. Cis-Trans Isomerization of Organic Molecules and Biomolecules: Implications and Applications. *Chem. Rev.* **2003**, *103*, 2475−2532.

(5) Bustamante, C.; Keller, D.; Oster, G. The Physics of Molecular Motors. *Acc. Chem. Res.* **2001**, *34*, 412−420.

(6) Feringa, B. L. In Control of Motion: From Molecular Switches to Molecular Motors. *Acc. Chem. Res.* **2001**, *34*, 504−513.

(7) Willner, I.; Willner, B. *Bioorganic Photochemistry: Biological Applications of Photochemical Switches*; Wiley: New York, 1993.

(8) Douhal, A.; Fiebig, T.; Chachisvilis, M.; Zewail, A. H. Femtochemistry in Nanocavities: Reactions in Cyclodextrins. *J. Phys. Chem. A* **1998**, *102*, 1657−1660.

(9) Zewail, A. H. Laser Femtochemistry. *Science* **1988**, *242*, 1645−1653.

(10) Cukier, R. I.; Nocera, D. G. Proton-Coupled Electron Transfer. *Annu. Rev. Phys. Chem.* **1998**, *49*, 337−369.

(11) Huynh, M. H. V.; Meyer, T. J. Proton-Coupled Electron Transfer. *Chem. Rev.* **2007**, *107*, 5004−5064.

(12) Hammes-Schiffer, S. Theoretical Perspectives on Proton-Coupled Electron Transfer Reactions. *Acc. Chem. Res.* **2001**, *34*, 273−281.

(13) Wang, T.; Brudvig, G. W.; Batista, V. S. Study of Proton Coupled Electron Transfer in a Biomimetic Dimanganese Water Oxidation Catalyst with Terminal Water Ligands. *J. Chem. Theory Comput.* **2010**, *6*, 2395−2401.

(14) Wang, T.; Brudvig, G.; Batista, V. S. Characterization of Proton Coupled Electron Transfer in a Biomimetic Oxomanganese Complex: Evaluation of the DFT B3LYP Level of Theory. *J. Chem. Theory Comput.* **2010**, *6*, 755−760.

(15) Hammes-Schiffer, S. Theory of Proton-Coupled Electron Transfer in Energy Conversion Processes. *Acc. Chem. Res.* **2009**, *42*, 1881−1889.

(16) Venkataraman, C.; Soudackov, A. V.; Hammes-Schiffer, S. Dynamics of Photoinduced Proton-Coupled Electron Transfer at Molecule-Semiconductor Interfaces: A Reduced Density Matrix Approach. *J. Phys. Chem. C* **2010**, *114*, 487−496.

(17) Auer, B.; Fernandez, L. E.; Hammes-Schiffer, S. Theoretical Analysis of Proton Relays in Electrochemical Proton-Coupled Electron Transfer. *J. Am. Chem. Soc.* **2011**, *133*, 8282−8292.

(18) Hammes-Schiffer, S. Current Theoretical Challenges in Proton-Coupled Electron Transfer: Electron-Proton Nonadiabaticity, Proton Relays, and Ultrafast Dynamics. *J. Phys. Chem. Lett.* **2011**, *2*, 1410−1416.

(19) Sirjoosingh, A.; Hammes-Schiffer, S. Diabatization Schemes for Generating Charge-Localized Electron-Proton Vibronic States in Proton-Coupled Electron Transfer Systems. *J. Chem. Theory Comput.* **2011**, *7*, 2831−2841.

(20) Sirjoosingh, A.; Hammes-Schiffer, S. Proton-Coupled Electron Transfer versus Hydrogen Atom Transfer: Generation of Charge-Localized Diabatic States. *J. Phys. Chem. A* **2011**, *115*, 2367−2377.

(21) Soudackov, A. V.; Hazra, A.; Hammes-Schiffer, S., Multidimensional Treatment of Stochastic Solvent Dynamics in Photoinduced Proton-Coupled Electron Transfer Processes: Sequential, Concerted, and Complex Branching Mechanisms. *J. Chem. Phys.* **2011**, *135*, 144115.

(22) Mayer, J. M.; Rhile, I. J. Thermodynamics and Kinetics of Proton-Coupled Electron Transfer: Stepwise vs. Concerted Pathways. *Biochimica et Biophysica Acta (BBA) - Bioenergetics* **2004**, *1655*, 51−58.

(23) Rhile, I. J.; Mayer, J. M. One-Electron Oxidation of a Hydrogen-Bonded Phenol Occurs by Concerted Proton-Coupled Electron Transfer. *J. Am. Chem. Soc.* **2004**, *126*, 12718−12719.

(24) Nibbering, E. T. J.; Fidder, H.; Pines, E. Ultrafast Chemistry: Using Time-Resolved Vibrational Spectroscopy for Interrogation of Structural Dynamics. *Annu. Rev. Phys. Chem.* **2005**, *56*, 337−367.

(25) Kukura, P.; McCamant, D. W.; Mathies, R. A. Femtosecond Stimulated Raman Spectroscopy. *Annu. Rev. Phys. Chem.* **2007**, *58*, 461−488.

(26) Elsaesser, T.; Kaiser, W. Visible and Infrared Spectroscopy of Intramolecular Proton Transfer Using Picosecond Laser Pulses. *Chem. Phys. Lett.* **1986**, *128*, 231−237.

(27) Moore, J. N.; Hansen, P. A.; Hochstrasser, R. M. Iron Carbonyl Bond Geometries of Carboxymyoglobin and Carboxyhemoglobin in Solution Determined by Picosecond Time-Resolved Infrared-Spectroscopy. *Proc. Natl. Acad. Sci. U.S.A.* **1988**, *85*, 5062−5066.

(28) Anfinrud, P. A.; Han, C.; Hochstrasser, R. M. Direct Observations of Ligand Dynamics in Hemoglobin by Subpicosecond Infrared-Spectroscopy. *Proc. Natl. Acad. Sci. U.S.A.* **1989**, *86*, 8387−8391.

(29) Yang, H.; Kotz, K. T.; Asplund, M. C.; Wilkens, M. J.; Harris, C. B. Ultrafast Infrared Studies of Bond Activation in Organometallic Completes. *Acc. Chem. Res.* **1999**, *32*, 551−560.

(30) Ridley, A. R.; Stewart, A. I.; Adamczyk, K.; Ghosh, H. N.; Kerkeni, B.; Guo, Z. X.; Nibbering, E. T. J.; Pickett, C. J.; Hunt, N. T. Multiple-Timescale Photoreactivity of a Model Compound Related to the Active Site of FeFe-Hydrogenase. *Inorg. Chem.* **2008**, *47*, 7453−7455.

(31) Lim, M.; Jackson, T. A.; Anfinrud, P. A. Binding of CO to Myoglobin from a Heme Pocket Docking Site to Form Nearly Linear Fe-C-O. *Science* **1995**, *269*, 962−966.

(32) Lim, M.; Jackson, T. A.; Anfinrud, P. A. Orientational Distribution of CO before and after Photolysis of MbCO and HbCO: A Determination Using Time-Resolved Polarized Mid-IR Spectroscopy. *J. Am. Chem. Soc.* **2004**, *126*, 7946−7957.

(33) Zemojtel, T.; Rini, M.; Heyne, K.; Dandekar, T.; Nibbering, E. T. J.; Kozlowski, P. M. NO-Bound Myoglobin: Structural Diversity and Dynamics of the NO Ligand. *J. Am. Chem. Soc.* **2004**, *126*, 1930−1931.

(34) Kim, S.; Lim, M. Picosecond Dynamics of Ligand Interconversion in the Primary Docking Site of Heme Proteins. *J. Am. Chem. Soc.* **2005**, *127*, 5786−5787.

(35) Chudoba, C.; Kummrow, A.; Dreyer, J.; Stenger, J.; Nibbering, E. T. J.; Elsaesser, T.; Zachariasse, K. A. Excited State Structure of 4-(Dimethylamino)benzonitrile Studied by Femtosecond Mid-Infrared Spectroscopy and Ab Initio Calculations. *Chem. Phys. Lett.* **1999**, *309*, 357−363.

(36) Okamoto, H. Picosecond Transient Infrared Spectrum of 4-(Dimethylamino)benzonitrile in the Fingerprint Region. *J. Phys. Chem. A* **2000**, *104*, 4182−4187.

(37) Okamoto, H.; Inishi, H.; Nakamura, Y.; Kohtani, S.; Nakagaki, R. Picosecond Infrared Spectra of Isotope-Substituted 4-(Dimethylamino)benzonitriles and Molecular Structure of the Charge-Transfer Singlet Excited State. *J. Phys. Chem. A* **2001**, *105*, 4182−4188.
(38) Okamoto, H.; Kinoshita, M.; Kohtani, S.; Nakagaki, R.; Zachariasse, K. A. Picosecond Infrared Spectra and Structure of Locally Excited and Charge Transfer Excited States of Isotope-Labeled 4-(Dimethylamino)benzonitriles. *Bull. Chem. Soc. Jpn.* **2002**, *75*, 957−963.
(39) Kwok, W. M.; Ma, C.; Phillips, D.; Matousek, P.; Parker, A. W.; Towrie, M. Picosecond Time-Resolved Study of 4-Dimethylaminobenzonitrile in Polar and Nonpolar Solvents. *J. Phys. Chem. A* **2000**, *104*, 4188−4197.
(40) Ma, C.; Kwok, W. M.; Matousek, P.; Parker, A. W.; Phillips, D.; Toner, W. T.; Towrie, M. Excited States of 4-Aminobenzonitrile (ABN) and 4-Dimethylaminobenzonitrile (DMABN): Time-Resolved Resonance Raman, Transient Absorption, Fluorescence, and Ab Initio Calculations. *J. Phys. Chem. A* **2002**, *106*, 3294−3305.
(41) Kwok, W. M.; Ma, C.; George, M. W.; Grills, D. C.; Matousek, P.; Parker, A. W.; Phillips, D.; Toner, W. T.; Towrie, M. Further Time-Resolved Spectroscopic Investigations on the Intramolecular Charge Transfer State of 4-Dimethylaminobenzonitrile (DMABN) and Its Derivatives, 4-Diethylaminobenzonitrile (DEABN) and 4-Dimethylamino-3,5-dimethylbenzonitrile (TMABN). *Phys. Chem. Chem. Phys.* **2003**, *5*, 1043−1050.
(42) Herbst, J.; Heyne, K.; Diller, R. Femtosecond Infrared Spectroscopy of Bacteriorhodopsin Chromophore Isomerization. *Science* **2002**, *297*, 822−825.
(43) Rini, M.; Holm, A.-K.; Nibbering, E. T. J.; Fidder, H. Ultrafast UV-Mid-IR Investigation of the Ring Opening Reaction of a Photochromic Spiropyran. *J. Am. Chem. Soc.* **2003**, *125*, 3028−3034.
(44) Fidder, H.; Rini, M.; Nibbering, E. T. J. The Role of Large Conformational Changes in Efficient Ultrafast Internal Conversion: Deviations from the Energy Gap Law. *J. Am. Chem. Soc.* **2004**, *126*, 3789−3794.
(45) Heyne, K.; Mohammed, O. F.; Usman, A.; Dreyer, J.; Nibbering, E. T. J.; Cusanovich, M. A. Structural Evolution of the Chromophore in the Primary Stages of Trans/Cis Isomerization in Photoactive Yellow Protein. *J. Am. Chem. Soc.* **2005**, *127*, 18100−18106.
(46) van Thor, J. J.; Ronayne, K. L.; Towrie, M. Formation of the Early Photoproduct Lumi-R of Cyanobacterial Phytochrome Cph1 Observed by Ultrafast Mid-Infrared Spectroscopy. *J. Am. Chem. Soc.* **2007**, *129*, 126−132.
(47) Mohammed, O. F.; Ahmed, S. A.; Vauthey, E.; Nibbering, E. T. J. Photoinduced Ring-Opening of a Photochromic Dihydroindolizine Derivative Monitored with Femtosecond Visible and Infrared Spectroscopy. *J. Phys. Chem. A* **2009**, *113*, 5061−5065.
(48) Mohammed, O. F.; Luber, S.; Batista, V. S.; Nibbering, E. T. J. Ultrafast Branching of Reaction Pathways in 2-(2′-Hydroxyphenyl)-benzothiazole in Polar Acetonitrile Solution. *J. Phys. Chem. A* **2011**, *115*, 7550−7558.
(49) Kukura, P.; McCamant, D. W.; Yoon, S.; Wandschneider, D. B.; Mathies, R. A. Structural Observation of the Primary Isomerization in Vision with Femtosecond-Stimulated Raman. *Science* **2005**, *310*, 1006−1009.
(50) Adesokan, A. A.; Pan, D.; Fredj, E.; Mathies, R. A.; Gerber, R. B. Anharmonic Vibrational Calculations Modeling the Raman Spectra of Intermediates in the Photoactive Yellow Protein (PYP) Photocycle. *J. Am. Chem. Soc.* **2007**, *129*, 4584−4594.
(51) Stuart, C. M.; Frontiera, R. R.; Mathies, R. A. Excited-State Structure and Dynamics of Cis- and Trans-Azobenzene from Resonance Raman Intensity Analysis. *J. Phys. Chem. A* **2007**, *111*, 12072−12080.
(52) Dasgupta, J.; Frontiera, R. R.; Taylor, K. C.; Lagarias, J. C.; Mathies, R. A. Ultrafast Excited-State Isomerization in Phytochrome Revealed by Femtosecond Stimulated Raman Spectroscopy. *Proc. Natl. Acad. Sci. U.S.A.* **2009**, *106*, 1784−1789.
(53) Takeuchi, S.; Ruhman, S.; Tsuneda, T.; Chiba, M.; Taketsugu, T.; Tahara, T. Spectroscopic Tracking of Structural Evolution in Ultrafast Stilbene Photoisomerization. *Science* **2008**, *322*, 1073−1077.
(54) Kuramochi, H.; Takeuchi, S.; Tahara, T. Ultrafast Structural Evolution of Photoactive Yellow Protein Chromophore Revealed by Ultraviolet Resonance Femtosecond Stimulated Raman Spectroscopy. *J. Phys. Chem. Lett.* **2012**, *3*, 2025−2029.
(55) Bredenbeck, J.; Helbing, J.; Hamm, P. Labeling Vibrations by Light: Ultrafast Transient 2D-IR Spectroscopy Tracks Vibrational Modes during Photoinduced Charge Transfer. *J. Am. Chem. Soc.* **2004**, *126*, 990−991.
(56) Mohammed, O. F.; Banerji, N.; Lang, B.; Nibbering, E. T. J.; Vauthey, E. Photoinduced Bimolecular Electron Transfer Investigated by Femtosecond Time-Resolved Infrared Spectroscopy. *J. Phys. Chem. A* **2006**, *110*, 13676−13680.
(57) Mohammed, O. F.; Adamczyk, K.; Banerji, N.; Dreyer, J.; Lang, B.; Nibbering, E. T. J.; Vauthey, E. Direct Femtosecond Observation of Tight and Loose Ion Pairs upon Photoinduced Bimolecular Electron Transfer. *Angew. Chem., Int. Ed.* **2008**, *47*, 9044−9048.
(58) Ghosh, H. N.; Verma, S.; Nibbering, E. T. J. Ultrafast Forward and Backward Electron Transfer Dynamics of Coumarin 337 in Hydrogen-Bonded Anilines as Studied with Femtosecond UV-Pump/IR-Probe Spectroscopy. *J. Phys. Chem. A* **2011**, *115*, 664−670.
(59) Rini, M.; Magnes, B. Z.; Pines, E.; Nibbering, E. T. J. Real-Time Observation of Bimodal Proton Transfer in Acid-Base Pairs in Water. *Science* **2003**, *301*, 349−352.
(60) Mohammed, O. F.; Pines, D.; Dreyer, J.; Pines, E.; Nibbering, E. T. J. Sequential Proton Transfer through Water Bridges in Acid-Base Reactions. *Science* **2005**, *310*, 83−86.
(61) Stoner-Ma, D.; Jaye, A. A.; Matousek, P.; Towrie, M.; Meech, S. R.; Tonge, P. J. Observation of Excited-State Proton Transfer in Green Fluorescent Protein Using Ultrafast Vibrational Spectroscopy. *J. Am. Chem. Soc.* **2005**, *127*, 2864−2865.
(62) van Thor, J. J.; Zanetti, G.; Ronayne, K. L.; Towrie, M. Structural Events in the Photocycle of Green Fluorescent Protein. *J. Phys. Chem. B* **2005**, *109*, 16099−16108.
(63) Stelling, A. L.; Ronayne, K. L.; Nappa, J.; Tonge, P. J.; Meech, S. R. Ultrafast Structural Dynamics in BLUF Domains: Transient Infrared Spectroscopy of AppA and Its Mutants. *J. Am. Chem. Soc.* **2007**, *129*, 15556−15564.
(64) Adamczyk, K.; Prémont-Schwarz, M.; Pines, D.; Pines, E.; Nibbering, E. T. J. Real-Time Observation of Carbonic Acid Formation in Aqueous Solution. *Science* **2009**, *326*, 1690−1694.
(65) van Thor, J. J. Photoreactions and Dynamics of the Green Fluorescent Protein. *Chem. Soc. Rev.* **2009**, *38*, 2935−2950.
(66) Meech, S. R. Excited State Reactions in Fluorescent Proteins. *Chem. Soc. Rev.* **2009**, *38*, 2922−2934.
(67) Fang, C.; Frontiera, R. R.; Tran, R.; Mathies, R. A. Mapping GFP Structure Evolution during Proton Transfer with Femtosecond Raman Spectroscopy. *Nature* **2009**, *462*, 200−204.
(68) Klöpffer, W. Intramolecular Proton Transfer in Electronically Excited Molecules. *Adv. Photochem.* **1977**, 311−358.
(69) Barbara, P. F.; Brus, L. E.; Rentzepis, P. M. Intramolecular Proton Transfer and Excited-State Relaxation in 2-(2-Hydroxyphenyl)-benzothiazole. *J. Am. Chem. Soc.* **1980**, *102*, 5631−5635.
(70) Chudoba, C.; Riedle, E.; Pfeiffer, M.; Elsaesser, T. Vibrational Coherence in Ultrafast Excited State Proton Transfer. *Chem. Phys. Lett.* **1996**, *263*, 622−628.
(71) Lochbrunner, S.; Wurzer, A. J.; Riedle, E. Ultrafast Excited-State Proton Transfer and Subsequent Coherent Skeletal Motion of 2-(2′-Hydroxyphenyl)benzothiazole. *J. Chem. Phys.* **2000**, *112*, 10699−10702.
(72) De Vivie-Riedle, R.; De Waele, V.; Kurtz, L.; Riedle, E. Ultrafast Excited-State Proton Transfer of 2-(2′-Hydroxyphenyl)benzothiazole: Theoretical Analysis of the Skeletal Deformations and the Active Vibrational Modes. *J. Phys. Chem. A* **2003**, *107*, 10591−10599.
(73) Barbatti, M.; Aquino, A. J. A.; Lischka, H.; Schriever, C.; Lochbrunner, S.; Riedle, E. Ultrafast Internal Conversion Pathway and Mechanism in 2-(2′-Hydroxyphenyl)benzathiazole: A Case Study for

Excited-State Intramolecular Proton Transfer Systems. *Phys. Chem. Chem. Phys.* **2009**, *11*, 1406−1415.
(74) Schriever, C.; Barbatti, M.; Stock, K.; Aquino, A. J. A.; Tunega, D.; Lochbrunner, S.; Riedle, E.; De Vivie-Riedle, R.; Lischka, H. The Interplay of Skeletal Deformations and Ultrafast Excited-State Intramolecular Proton Transfer: Experimental and Theoretical Investigation of 10-Hydroxybenzo[h]quinoline. *Chem. Phys.* **2008**, *347*, 446−461.
(75) Aquino, A. J. A.; Lischka, H.; Hättig, C. Excited-State Intramolecular Proton Transfer: A Survey of TDDFT and RI-CC2 Excited-State Potential Energy Surfaces. *J. Phys. Chem. A* **2005**, *109*, 3201−3208.
(76) Lochbrunner, S.; Wurzer, A. J.; Riedle, E. Microscopic Mechanism of Ultrafast Excited-State Intramolecular Proton Transfer: A 30-fs Study of 2-(2′-Hydroxyphenyl)benzothiazole. *J. Phys. Chem. A* **2003**, *107*, 10580−10590.
(77) Kim, Y. H.; Roh, S.-G.; Jung, S.-D.; Chung, M.-A.; Kim, H. K.; Cho, D. W. Excited-State Intramolecular Proton Transfer on 2-(2'-Hydroxy-4'-R-Phenyl) Benzothiazole Nanoparticles and Fluorescence Wavelength Depending on Substituent and Temperature. *Photochem. Photobiol. Sci.* **2010**, *9*, 722−729.
(78) Formosinho, S. J.; Arnaut, L. G. Excited-State Proton-Transfer Reactions. II. Intramolecular Reactions. *J. Photochem. Photobiol., A* **1993**, *75*, 21−48.
(79) Elsaesser, T. Ultrafast Excited State Hydrogen Transfer in the Condensed Phase. In *Ultrafast hydrogen Bonding Dynamics and Proton Transfer Processes in the Condensed Phase*; Elsaesser, T., Bakker, H. J., Eds.; Kluwer Academic Publishers: Dordrecht, The Netherlands, 2002; pp 119−153.
(80) Tsai, H.-H. G.; Sun, H.-L. S.; Tan, C.-J. TD-DFT Study of the Excited-State Potential Energy Surfaces of 2-(2′-Hydroxyphenyl)-benzimidazole and Its Amino Derivatives. *J. Phys. Chem. A* **2010**, *114*, 4065−4079.
(81) Xiao-Ming, W.; Yu-Lin, H.; Zhao-Qi, W.; Jia-Jin, Z.; Xiu-Lan, F.; Yuan-Yuan, S. White Organic Light-Emitting Devices Based on 2-(2-Hydroxyphenyl)benzothiazole and Its Chelate Metal Complex. *Chin. Phys. Lett.* **2005**, *22*, 1797−1799.
(82) Chang, S. M.; Tzeng, Y. J.; Wu, S. Y.; Li, K. Y.; Hsueh, K. L. Emission of White Light from 2-(2′-Hydroxyphenyl)benzothiazole in Polymer Electroluminescent Devices. *Thin Solid Films* **2005**, *477*, 38−41.
(83) Hao, Y.; Meng, W.; Xu, H.; Wang, H.; Liu, X.; Xu, B. White Organic Light-Emitting Diodes Based on a Novel Zn Complex with High CRI Combining Emission from Excitons and Interface-Formed Electroplex. *Org. Electron.* **2011**, *12*, 136−142.
(84) Huixia, X.; Bingshe, X.; Xiaohong, F.; Liuqing, C.; Hua, W.; Yuying, H. Correlation between Molecular Structure and Optical Properties for the Bis(2-(2-hydroxyphenyl)benzothiazolate) Complexes. *J. Photochem. Photobiol., A* **2011**, *217*, 108−116.
(85) Yu, G.; Yin, S.; Liu, Y.; Shuai, Z.; Zhu, D. Structures, Electronic States, and Electroluminescent Properties of a Zinc(II) 2-(2-Hydroxyphenyl)benzothiazolate Complex. *J. Am. Chem. Soc.* **2003**, *125*, 14816−14824.
(86) Yang, Y.; Geng, H.; Shuai, Z.; Peng, J. First-Principles Electronic Structure of Light-Emitting and Transport Materials: Zinc(II)2-(2-hydroxyphenyl)benzothiazole. *Synth. Met.* **2006**, *156*, 1287−1291.
(87) Kwak, M. J.; Kim, Y. Photostable BF2-Chelated Fluorophores Based on 2-(2′-Hydroxyphenyl)benzoxazole and 2-(2′-Hydroxyphenyl)benzothiazole. *Bull. Korean Chem. Soc.* **2009**, *30*, 2865−2866.
(88) Xu, H.; Xu, B.; Fang, X.; Yue, Y.; Chen, L.; Wang, H.; Hao, Y. Molecular Structure, Photoluminescent and Electroluminescent Properties of Bis(2-(4-methyl-2-hydroxyphenyl) benzothiazolate) Zinc with Excellent Electron-Transport Characteristics. *Mater. Chem. Phys.* **2011**, *129*, 840−845.
(89) Qian, Y.; Li, S.; Wang, Q.; Zhang, G.; Wang, S.; Xu, H.; Li, C.; Li, Y.; Yang, G. Aggregation-Induced Emission Enhancement of 2-(2′-Hydroxyphenyl)benzothiazole-Based Excited-State Intramolecular Proton-Transfer Compounds. *J. Phys. Chem. B* **2007**, *111*, 5861−5868.
(90) Yao, D.; Zhao, S.; Guo, J.; Zhang, Z.; Zhang, H.; Liu, Y.; Wang, Y. Hydroxyphenyl-Benzothiazole Based Full Color Organic Emitting Materials Generated by Facile Molecular Modification. *J. Mater. Chem.* **2011**, *21*, 3568−3570.
(91) Wang, R.; Liu, D.; Xu, K.; Li, J. Substituent and Solvent Effects on Excited State Intramolecular Proton Transfer in Novel 2-(2′-Hydroxyphenyl)Benzothiazole Derivatives. *J. Photochem. Photobiol., A* **2009**, *205*, 61−69.
(92) Bingshe, X.; Huixia, X.; Liuqing, C.; Xiaohong, F.; Xuguang, L.; Hua, W. Effects of Methyl Substitution of Metal (II) Bis(2-(2-hydroxyphenyl)benzothiazolate) Chelates on Optical Properties. *Org. Electron.* **2008**, *9*, 267−272.
(93) Rodembusch, F. S.; Leusin, F. P.; Campo, L. F.; Stefani, V. Excited State Intramolecular Proton Transfer in Amino 2-(2′-Hydroxyphenyl)benzazole Derivatives: Effects of the Solvent and the Amino Group Position. *J. Lumin.* **2007**, *126*, 728−734.
(94) Sepiol, J.; Grabowska, A.; Borowicz, P.; Kijak, M.; Broquier, M.; Jouvet, C.; Dedonder-Lardeux, C.; Zehnacker-Rentien, A. Excited-State Intramolecular Proton Transfer Reaction Modulated by Low-Frequency Vibrations: An Effect of an Electron-Donating Substituent on the Dually Fluorescent Bis-Benzoxazole. *J. Chem. Phys.* **2011**, *135*, 034307.
(95) Sobolewski, A. L.; Domcke, W. Intramolecular Hydrogen Bonding in the S1(pi pi*) Excited State of Anthranilic Acid and Salicylic Acid: TDDFT Calculation of Excited-State Geometries and Infrared Spectra. *J. Phys. Chem. A* **2004**, *108*, 10917−10922.
(96) Furche, F.; Ahlrichs, R. Adiabatic Time-Dependent Density Functional Methods for Excited State Properties. *J. Chem. Phys.* **2002**, *117*, 7433−7447.
(97) Hutter, J. Excited State Nuclear Forces from the Tamm-Dancoff Approximation to Time-Dependent Density Functional Theory within the Plane Wave Basis Set Framework. *J. Chem. Phys.* **2003**, *118*, 3928−3934.
(98) Gonzalez, L.; Escudero, D.; Serrano-Andrés, L. Progress and Challenges in the Calculation of Electronic Excited States. *ChemPhysChem* **2012**, *13*, 28−51.
(99) Roos, B. O. Perspectives in Calculations on Excited States in Molecular Systems. *Computational Photochemistry*; Elsevier: Amsterdam, The Netherlands, 2005; pp 317−348.
(100) Dreyer, J.; Kummrow, A. Shedding Light on Excited-State Structures by Theoretical Analysis of Femtosecond Transient Infrared Spectra: Intramolecular Charge Transfer in 4-(Dimethylamino)-benzonitrile. *J. Am. Chem. Soc.* **2000**, *122*, 2577−2585.
(101) Jas, G. S.; Kuczera, K. Ab Initio Calculations of S1 Excited State Vibrational Spectra in Benzene, Napthalene and Anthracene. *Chem. Phys.* **1997**, *214*, 229−241.
(102) van Thor, J. J.; Ronayne, K. L.; Towrie, M.; Sage, J. T. Balance between Ultrafast Parallel Reactions in the Green Fluorescent Protein Has a Structural Origin. *Biophys. J.* **2008**, *95*, 1902−1912.
(103) Usman, A.; Mohammed, O. F.; Nibbering, E. T. J.; Dong, J.; Solntsev, K. M.; Tolbert, L. M. Excited-State Structure Determination of the Green Fluorescent Protein Chromophore. *J. Am. Chem. Soc.* **2005**, *127*, 11214−11215.
(104) Stoner-Ma, D.; Melief, E. H.; Nappa, J.; Ronayne, K. L.; Tonge, P. J.; Meech, S. R. Proton Relay Reaction in Green Fluorescent Protein (GFP): Polarization-Resolved Ultrafast Vibrational Spectroscopy of Isotopically Edited GFP. *J. Phys. Chem. B* **2006**, *110*, 22009−22018.
(105) Szabo, A. Theory of Fluorescence Depolarization in Macromolecules and Membranes. *J. Chem. Phys.* **1984**, *81*, 150−167.
(106) Lin, Y.-S.; Pieniazek, P. A.; Yang, M.; Skinner, J. L. On the Calculation of Rotational Anisotropy Decay, as Measured by Ultrafast Polarization-Resolved Vibrational Pump-Probe Experiments. *J. Chem. Phys.* **2010**, *132*, 174505.
(107) Van Wilderen, L. J. G. W.; Lincoln, C. N.; Van Thor, J. J. Modelling Multi-Pulse Population Dynamics from Ultrafast Spectroscopy. *PLOS ONE* **2011**, *6*, e17373.
(108) Chachisvilis, M.; Fidder, H.; Sundström, V. Electronic Coherence in Pseudo Two-Colour Pump-Probe Spectroscopy. *Chem. Phys. Lett.* **1995**, *234*, 141−150.

(109) Wynne, K.; Hochstrasser, R. M. The Theory of Ultrafast Vibrational Spectroscopy. *Chem. Phys.* **1995**, *193*, 211−236.
(110) Hamm, P. Coherent Effects in Femtosecond Infrared Spectroscopy. *Chem. Phys.* **1995**, *200*, 415−429.
(111) Rini, M.; Kummrow, A.; Dreyer, J.; Nibbering, E. T. J.; Elsaesser, T. Femtosecond Mid-Infrared Spectroscopy of Condensed Phase Hydrogen-Bonded Systems as a Probe of Structural Dynamics. *Faraday Discuss.* **2003**, *122*, 27−40.
(112) Rini, M.; Dreyer, J.; Nibbering, E. T. J.; Elsaesser, T. Ultrafast Vibrational Relaxation Processes Induced by Intramolecular Excited State Hydrogen Transfer. *Chem. Phys. Lett.* **2003**, *374*, 13−19.
(113) Scalmani, G.; Frisch, M. J., Continuous Surface Charge Polarizable Continuum Models of Solvation. I. General Formalism. *J. Chem. Phys.* **2010**, *132*, 114110.
(114) Frisch, M. J.; Trucks, G. W.; Schlegel, H. B.; Scuseria, G. E.; Robb, M. A.; Cheeseman, J. R.; Scalmani, G.; Barone, V.; Mennucci, B.; Petersson, G. A.; et al. *Gaussian 09*; Gaussian, Inc.: Wallingford, CT, 2009.
(115) Neugebauer, J.; Reiher, M.; Kind, C.; Hess, B. A. Quantum Chemical Calculation of Vibrational Spectra of Large Molecules - Raman and IR Spectra for Buckminsterfullerene. *J. Comput. Chem.* **2002**, *23*, 895−910.
(116) Neugebauer, J.; Herrmann, C.; Luber, S.; Reiher, M. *SNF 4.0 — A Program for the Quantum Chemical Calculation of Vibrational Spectra*, 2010.
(117) Becke, A. D. Density-Functional Exchange-Energy Approximation with Correct Asymptotic Behavior. *Phys. Rev. A* **1988**, *38*, 3098−3100. Perdew, J. P. Density-Functional Approximation for the Correlation Energy of the Inhomogeneous Electron Gas. *Phys. Rev. B* **1986**, *33*, 8822−8824.
(118) Becke, A. D. Density-Functional Thermochemistry III. The Role of Exact Exchange. *J. Chem. Phys.* **1993**, *98*, 5648−5652.
(119) Lee, C.; Yang, W.; Parr, R. G. Development of the Colle-Salvetti Correlation-Energy Formula into a Functional of the Electron-Density. *Phys. Rev. B* **1988**, *37*, 785−789.
(120) Schäfer, A.; Horn, H.; Ahlrichs, R. Fully Optimized Contracted Gaussian-Basis Sets for Atoms Li to Kr. *J. Chem. Phys.* **1992**, *97*, 2571−2577.
(121) Schäfer, A.; Huber, C.; Ahlrichs, R. Fully Optimized Contracted Gaussian-Basis Sets of Triple Zeta Valence Quality for Atoms Li to Kr. *J. Chem. Phys.* **1994**, *100*, 5829−5835.
(122) Dunning, T. H., Jr. Gaussian Basis Sets for Use in Correlated Molecular Calculations: I. The Atoms Boron through Neon and Hydrogen. *J. Chem. Phys.* **1989**, *90*, 1007−1023.
(123) Ahlrichs, R.; Bär, M.; Häser, M.; Horn, H.; Kölmel, C. Electronic Structure Calculations on Workstation Computers: The Program System Turbomole. *Chem. Phys. Lett.* **1989**, *162*, 165−169.
(124) Bickley, W. G. Formulae for Numerical Differentiation. *Math. Gaz.* **1941**, *25*, 19−27.
(125) Singh, U. C.; Kollman, P. A. An Approach to Computing Electrostatic Charges for Molecules. *J. Comput. Chem.* **1984**, *5*, 129−145.
(126) Besler, B. H.; Merz, K. M., Jr.; Kollman, P. A. Atomic Charges Derived from Semiempirical Methods. *J. Comput. Chem.* **1990**, *11*, 431−439.
(127) Humphrey, W.; Dalke, A.; Schulten, K. VMD: Visual Molecular Dynamics. *J. Mol. Graphics* **1996**, *14*, 33−38.
(128) Hanson, R. M. Jmol - A Paradigm Shift in Crystallographic Visualization. *J. Appl. Crystallogr.* **2010**, *43*, 1250−1260.
(129) Guallar, V.; Batista, V. S.; Miller, W. H. Semiclassical Molecular Dynamics Simulations of Intramolecular Proton Transfer in Photo-excited 2-(2′-Hydroxyphenyl)-oxazole. *J. Chem. Phys.* **2000**, *113*, 9510−9522.
(130) Kim, J.; Wu, Y. H.; Brédas, J. L.; Batista, V. S. Quantum Dynamics of the Excited-State Intramolecular Proton Transfer in 2-(2′-Hydroxyphenyl)benzothiazole. *Isr. J. Chem.* **2009**, *49*, 187−197.